

# Fabrication and characterization of electrospun Ag doped TiO<sub>2</sub> nanofibers for photocatalytic reaction

Ju-Young Park · Kyung-Jun Hwang ·  
Jae-Wook Lee · In-Hwa Lee

Received: 11 October 2010 / Accepted: 1 June 2011 / Published online: 28 June 2011  
© Springer Science+Business Media, LLC 2011

**Abstract** Titanium dioxide is one of the best semiconductor photocatalysts available for photocatalytic reaction of dye pollutants. To prevent the recombination caused by the relatively low photocatalytic efficiency, Ag doped TiO<sub>2</sub> nanofiber was prepared by electrospinning method. The photocatalysts (pure TiO<sub>2</sub> nanofiber and Ag doped TiO<sub>2</sub> nanofiber) were characterized by FE-SEM, XRD, XPS, and PL analysis. These photocatalysts were evaluated by the photodecomposition of methylene blue under UV light. Ag doped TiO<sub>2</sub> nanofiber was found to be more efficient than pure TiO<sub>2</sub> fiber for photocatalytic degradation of methylene blue. The photocatalytic degradation rate was applied to pseudo-first-order equation. The degradation of Ag doped TiO<sub>2</sub> nanofiber was significantly higher than the degradation rate of pure TiO<sub>2</sub> nanofiber. Activation energy was calculated by applying Arrhenius equation from the rate constant of photocatalytic reaction. The activation energies for the pure TiO<sub>2</sub> nanofibers calcined at 400 and 500 °C were 16.981 and 12.187 kJ/mol and those of Ag

doped TiO<sub>2</sub> nanofibers were 18.317 and 7.977 kJ/mol, respectively.

## Introduction

Titanium dioxide (TiO<sub>2</sub>) is one of the metal oxide semiconductors that has been considerably investigated and utilized in a wide range of applications such as catalytic devices, solar cells, sensors, and other optoelectronic devices [1–5]. It was also well known for its remarkable photocatalytic properties. TiO<sub>2</sub> is known to have three crystalline phases of anatase, rutile, and brookite. It was reported that the physical characteristics of TiO<sub>2</sub>, including crystallization, grain size, morphology, surface area, surface state, and porosity, clearly influence the photocatalytic activity of TiO<sub>2</sub> [6–10]. Moreover, some metal materials, such as Ag, Pd, and Pt, supported on the TiO<sub>2</sub> surface can greatly accelerate the decomposition rate of organic compound by effectively consuming the photo-produced electrons in the reduction of oxygen, thereby reducing the recombination of electrons ( $e^-$ ) and holes ( $h^+$ ) [11–16].

Electrospinning is one of the simple and versatile methods for generating TiO<sub>2</sub> fibers when combined with the sol–gel process. The fabrication of TiO<sub>2</sub> fibers by electrospinning was first reported in 2003 [17]. Chuangchote et al. [18–20] have already prepared pure inorganic fibers comprising the TiO<sub>2</sub>. On the basis of these previous reports, titania fibers were electrospun from a mixture of titanium propoxide (TiP) and polymer. After thermal treatment, titanium oxide (anatase and/or rutile phase) fibers were obtained. Zhou et al. [21–23] have studied electrospun TiO<sub>2</sub> fiber as the photocatalyst to be applied for application to the degradation of dye pollutants. Unfortunately, there are hardly any research on

J.-Y. Park  
Department of Physics and Astronomy, Seoul National University, Seoul 151-747, Republic of Korea

J.-Y. Park · I.-H. Lee  
Department of Environmental Engineering, BK21 Team for Biohydrogen Production, Chosun University, Gwangju 501-759, Republic of Korea

J.-Y. Park (✉)  
Southwestern Research Institute of Green Energy Technology, Mokpo-Si, Jeollanam-do 530-400, Republic of Korea  
e-mail: gom8812@hanmail.net

K.-J. Hwang · J.-W. Lee  
Department of Chemical and Biochemical Engineering, Chosun University, Gwangju 501-759, Republic of Korea

photocatalyst degradation using metal doped (Ag, Pd, and Pt)  $\text{TiO}_2$  nanofiber.

In this study, to prevent the recombination caused by of the relatively low photocatalytic efficiency, Ag doped  $\text{TiO}_2$  nanofibers were prepared by electrospinning method. The sample of photocatalysts (pure  $\text{TiO}_2$  nanofiber and Ag doped  $\text{TiO}_2$  nanofiber) were characterized by conducting FE-SEM, XRD, XPS, and PL analysis. The photocatalysts were evaluated for the photodecomposition of methylene blue under UV light. The reaction rate ( $k$ ) constant and activation energy ( $E_a$ ) were evaluated from the experimental data of photocatalytic reaction.

## Experimental

### Materials

Poly(vinyl pyrrolidone) (PVP) (PVP; Mw = 1,300,000) and titanium isopropoxide (TiP) were obtained from Aldrich Company. Silver nitrate ( $\text{AgNO}_3$ ), acetic acid, and ethanol were purchased from Dajung. These chemicals were used without further purification.

### Preparation of $\text{TiO}_2$ nanofibers

To date, a few reports have dealt with electrospinning of precursor solutions that could lead to the formation of composite fiber [24]. TiP (a sol–gel precursor to titania) can be directly added to an alcohol solution containing PVP. To suppress the hydrolysis reaction of the sol–gel precursor, acetic acid as well as PVP solution in ethanol must be added. In a typical procedure, 6 mL of TiP was mixed with 12 mL of acetic acid and 12 mL of ethanol. After 60 min, this solution was added to 30 g of ethanol that contained 10 wt% PVP and 2.5%  $\text{AgNO}_3$  of TiP followed by magnetic stirring for 24 h (with the solution held in a capped bottle). The mixture was immediately loaded into a glass syringe equipped with a 21 G needle made of stainless steel. The needle was connected to a high voltage supply (DC power supply PS/ER 50R06 DM22, Glassman High Voltage Inc., USA) that is capable of generating DC voltages up to 50 kV. A voltage of 20 kV was applied between the needle and the collector. The distance between the needle and the target was 15 cm. A flow rate of 50  $\mu\text{L}/\text{min}$  was maintained using a syringe. Electrospinning process was carried out the room temperature.  $\text{TiO}_2$  nanofibers were calcined at 450 and 500 °C for 4 h.

### Characterization of $\text{TiO}_2$ fibers

The morphology of electrospun fiber was observed on a field emission scanning electron microscopy (FE-SEM)

(Hitach, S-4800). X-ray diffraction (XRD) pattern was recorded using a Philips (X’Pert PRO MPO) diffractometer ( $\text{Cu K}\alpha$  radiation) at a scanning rate of 0.01°/s in  $2\theta$  ranging from 10° to 90°. XPS analysis was conducted using a photoelectron spectrometer VG Scientifical MultiLab 2000 system equipped with a non-monochromatic  $\text{Mg K}\alpha$  radiation. All binding energies (BE) were calibrated by the BE (284.6 eV) of C1s, which gave BE values within an accuracy of +0.1 eV. The PL spectra were recorded on PE LS55 FS spectrometer, with an excitation wavelength of 300 nm.

### Photocatalytic activity

Photocatalytic degradation of methylene blue solution was performed by placing a 500 mL quartz tube in the middle of four 8 W shortwave UV lamps (254 nm) (Philips, USA), and the distance between two lamps is 5 cm. The UV lamp was positioned inside a cylindrical Pyrex vessel and surrounded by a circulating water jacket to remove the heat. 50 mg photocatalyst (pure  $\text{TiO}_2$  nanofiber and Ag doped  $\text{TiO}_2$  nanofiber) and 10.0 mg/L of methylene blue were added to the quartz tube. The photocatalyst was extended well in the methylene blue solution without stirring. Prior to irradiation, the photocatalytic reaction system was stirred in a dark condition for 10 min to establish an adsorption–desorption equilibrium condition. The photocatalytic reaction system was sampled at regular intervals. The remaining methylene blue concentration after adsorption–desorption equilibrium ( $C_0$ ) and during the photodegradation ( $C$ ) was detected by UV/VIS at 660 nm. The degradation efficiency was expressed by  $(C/C_0)$ .

## Results and discussion

The pure  $\text{TiO}_2$  nanofiber and Ag doped  $\text{TiO}_2$  nanofiber at different calcination temperatures are shown in Fig. 1. The surface of Ag doped  $\text{TiO}_2$  nanofiber is smoother than that of  $\text{TiO}_2$  nanofiber and the grain size of the fiber is smaller. This phenomenon can be explained by the fact that the silver suppressed the phase transition and the size of a single crystal was reduced. The diameter of the calcinated nanofiber is smaller than that of the as-spun fibers because of the shrinkage caused by loss of ethanol, degradation of PVP, decomposition of TiP, and the succeeding sintering [22].

Figure 2 shows XRD pattern of pure  $\text{TiO}_2$  nanofiber and Ag doped  $\text{TiO}_2$  nanofiber at calcination temperature. The pure  $\text{TiO}_2$  nanofiber has both anatase and rutile phase, while Ag doped  $\text{TiO}_2$  nanofiber has only the anatase phase. From these results, we found that silver decreases the phase transition temperature. There were two possible reasons for the decrease in the phase transformation temperature. One

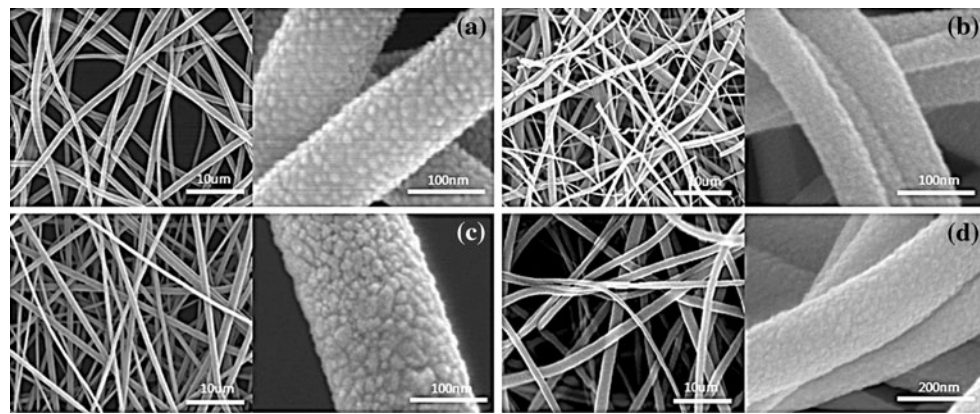


**Fig. 1** FE-SEM image of pure  $\text{TiO}_2$  nanofiber and Ag doped  $\text{TiO}_2$  nanofiber: **a**  $\text{TiO}_2$  nanofiber ( $450\text{ }^\circ\text{C}$ ), **b** Ag doped  $\text{TiO}_2$  nanofiber ( $450\text{ }^\circ\text{C}$ ), **c**  $\text{TiO}_2$  nanofiber ( $500\text{ }^\circ\text{C}$ ), **d** Ag doped  $\text{TiO}_2$  nanofibers ( $500\text{ }^\circ\text{C}$ )

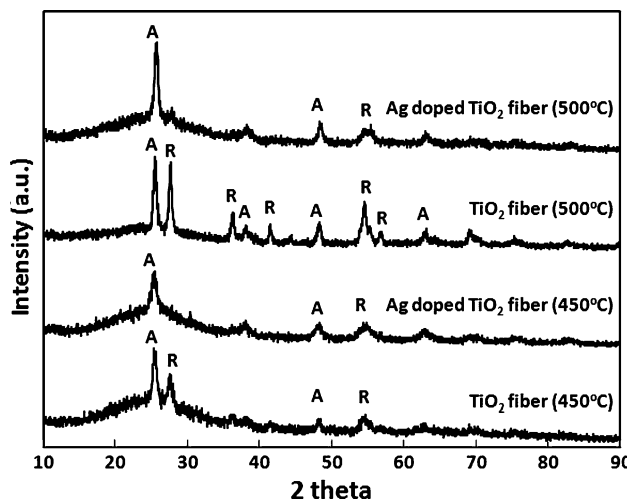


**Fig. 2** XRD pattern of pure  $\text{TiO}_2$  nanofiber and Ag doped  $\text{TiO}_2$  nanofiber at different calcination temperature

was that the density of surface defects of Ag doped  $\text{TiO}_2$  nanofiber would increase with the increase Ag doping content, which would promote the phase transformation

because the surface defects were considered as the rutile nucleation sites [25, 26]. The other reason that the surface oxygen vacancy concentration of anatase grains is increased with an increase in the Ag dopant content [27], which favored the rearrangement of ions and reorganization of the structure for rutile phase. Thus, Ag dopant retained the anatase to rutile phase transformation.

As shown in Table 1, the size of average crystals (anatase and rutile) of Ag doped  $\text{TiO}_2$  nanofiber is smaller than pure  $\text{TiO}_2$  nanofiber because silver controls the phase transformation. In other words, it can be seen that the phase transformation temperature of  $\text{TiO}_2$  nanofiber in the Ag doped  $\text{TiO}_2$  nanofiber catalyst from anatase to rutile went down, and the anatase crystallinity was hindered as silver was doped.

Figure 3 shows the typical XPS survey spectra of pure  $\text{TiO}_2$  nanofiber and Ag doped  $\text{TiO}_2$  nanofiber. It is observed that pure  $\text{TiO}_2$  nanofiber consists of the Ti, O, and C element; and the binding energies of  $\text{Ti}2\text{p}1$ ,  $\text{Ti}2\text{p}3$ ,  $\text{O}1\text{s}$ , and  $\text{C}1\text{s}$  are 464.1, 458.4, 529.6, and 284.6 eV, respectively, while Ag doped  $\text{TiO}_2$  nanofiber contains Ag in addition to two elements above elements because of the

**Table 1** Diameter of physical properties of precalcined as-spun  $\text{TiO}_2/\text{PVP}$  composite nanofiber and calcined  $\text{TiO}_2$  nanofiber at different temperature

Material	Calcination temperature ( $^\circ\text{C}$ )	Percentage of the anatase phase <sup>a</sup>	Size of the anatase crystals <sup>b</sup> (nm)	Size of the rutile crystals <sup>c</sup> (nm)	Size of average crystals
$\text{TiO}_2$ nanofiber	Precalcined	—	—	—	—
$\text{TiO}_2$ nanofiber	450	67	10.95	11.00	10.96
$\text{TiO}_2$ nanofiber	500	46	15.33	28.83	13.99
Ag doped $\text{TiO}_2$ nanofiber	Precalcined	—	—	—	—
Ag doped $\text{TiO}_2$ nanofiber	450	100	6.39	—	6.39
Ag doped $\text{TiO}_2$ nanofiber	500	100	10.95	—	10.95

<sup>a</sup> Calculated based on the procedure given by Cullity et al. [28]

<sup>b,c</sup> Calculated by the Scherrer equation

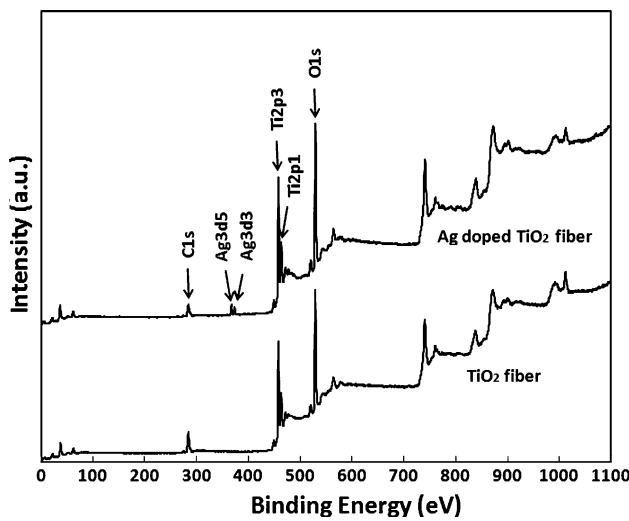


**Fig. 3** XPS survey spectra of pure TiO<sub>2</sub> nanofiber and Ag doped TiO<sub>2</sub> nanofiber prepared at 500 °C

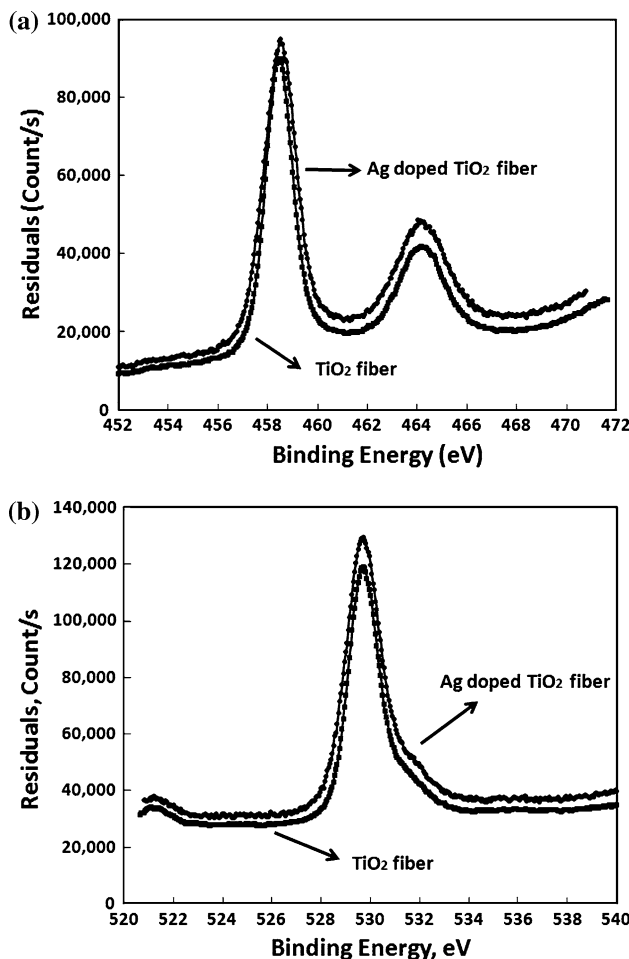


**Fig. 4** XPS spectrum (Ti2p and O1s) of pure TiO<sub>2</sub> nanofiber and Ag doped TiO<sub>2</sub> nanofiber prepared at 500 °C

presence of Ag3d3 and Ag3d5 peaks. The binding energies of Ag3d3 and Ag3d5 peaks are 367.5 and 373.7.

Figure 4 presents the results of the quantitative XPS analysis of pure TiO<sub>2</sub> nanofiber and Ag doped TiO<sub>2</sub> nanofiber. The Ti2p<sub>1</sub> and Ti2p<sub>3</sub> spin-orbital splitting photoelectrons of pure TiO<sub>2</sub> nanofibers are located at the binding energies of 464.2 and 458.4 eV. The O1s peak of pure TiO<sub>2</sub> nanofiber is shown at 529.6 eV and a shoulder is located toward the side of higher binding energies. The contents of Ti and O of pure TiO<sub>2</sub> nanofiber are 38.9 and 61.1%. Also, the contents of Ti and O of Ag doped TiO<sub>2</sub> nanofiber are 38.2 and 61.8%. As shown in Fig. 4, the Ti2p binding energy of the Ag doped TiO<sub>2</sub> nanofiber is increased as compared to that of pure TiO<sub>2</sub> nanofiber because the Fermi level of Ag is lower than that of TiO<sub>2</sub> nanofiber so that the conduction band electrons of TiO<sub>2</sub> nanofiber are

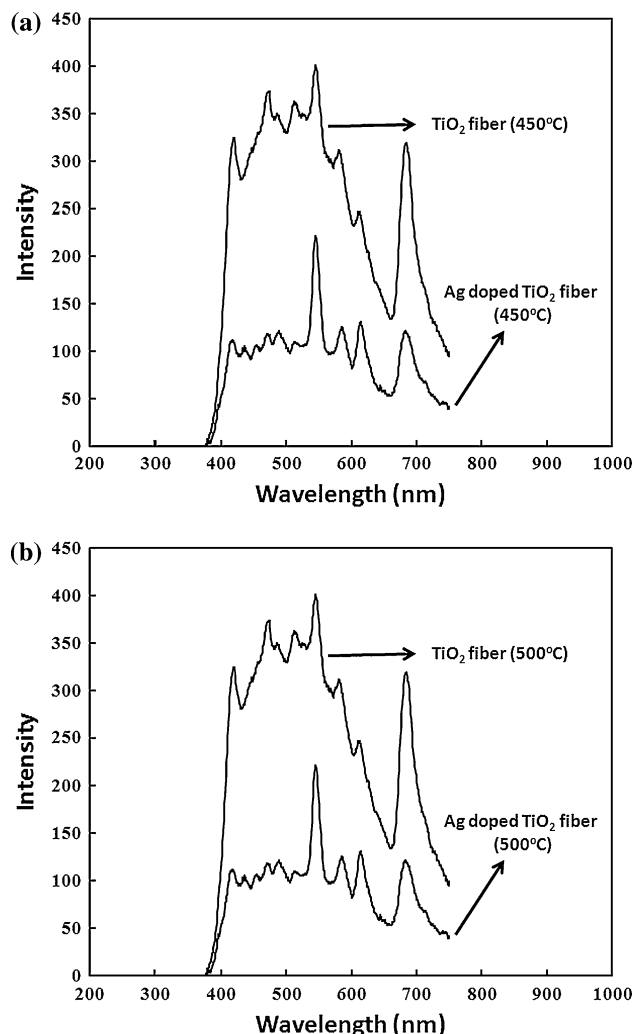


**Fig. 5** PL spectra of pure TiO<sub>2</sub> nanofiber and Ag doped TiO<sub>2</sub> fiber at different calcination temperature ( $\lambda_{\max} = 300$  nm): **a** 450 °C, **b** 500 °C

transferred to the Ag doped on the surface of  $\text{TiO}_2$  fiber, which results in a decrease in the out electron cloud density of Ti ion [11].

The optical properties of solid materials are closely related to their microstructure, such as electronic state, defect state, and energy level structure [29]. The PL spectra are related to the transfer behavior of the photoinduced electrons and holes so that they can reflect the separation and recombination of photoinduced charge carrier, thus it is used to primarily evaluate the recombination rate of charge carriers [30]. As shown in Fig. 5, the PL intensity of Ag doped  $\text{TiO}_2$  nanofiber is lower than pure  $\text{TiO}_2$  nanofiber. Ag ions are diffused into the crystal lattice of  $\text{TiO}_2$  nanofiber, and the  $\text{Ag}^{\circ}$  deposited on the surface can act as traps to capture the photoinduced electron, inhibiting the recombination of electron–hole pairs so as to make PL single decrease [11].

Figure 6 indicates the changes MB concentration with pure  $\text{TiO}_2$  nanofiber and Ag doped  $\text{TiO}_2$  nanofiber versus the irradiation time. As to the MB solution with both catalysts, the concentration of MB is significantly decreased. A comparative analysis shows clearly that the decrease rate of the concentration of MB with Ag doped  $\text{TiO}_2$  nanofiber as catalyst is higher than that of pure  $\text{TiO}_2$  nanofiber as catalyst. Under the same reaction condition, photodegradation efficiency of catalysts was affected by reaction temperature.

**Fig. 6** Photocatalytic degradation of the methylene blue with UV irradiation: **a** pure  $\text{TiO}_2$  nanofiber ( $450\text{ }^{\circ}\text{C}$ ), **b** Ag doped  $\text{TiO}_2$  nanofiber ( $450\text{ }^{\circ}\text{C}$ ), **c** pure  $\text{TiO}_2$  nanofiber ( $500\text{ }^{\circ}\text{C}$ ), **d** Ag doped  $\text{TiO}_2$  nanofiber ( $500\text{ }^{\circ}\text{C}$ )

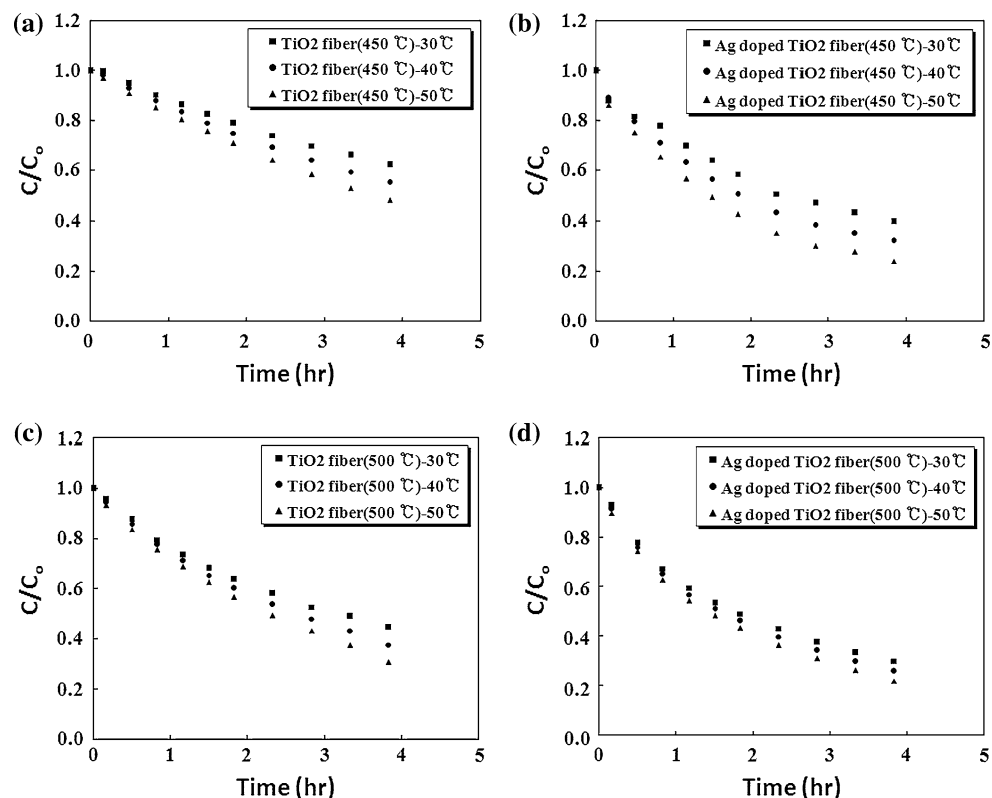


Table 2 presents the results of removal efficiency of methylene blue by photocatalytic degradation at different temperature after reaction time 3 h. Ag doped  $\text{TiO}_2$  nanofiber showed a higher efficiency than pure  $\text{TiO}_2$  nanofiber regardless of the calcination temperature. The removal efficiency was high at the calcination temperature of  $500\text{ }^{\circ}\text{C}$ . In the case of Ag doped  $\text{TiO}_2$  nanofiber, the degradation ratio was the highest, which may have been attributed to the following four reasons: (1) Appropriate amount of the doped and deposited Ag species on the surface layer of  $\text{TiO}_2$  nanofiber effectively captured the photoinduced electrons and holes. (2) Photoinduced electrons were quickly transferred to the oxygen adsorbed on the surface of  $\text{TiO}_2$  nanofiber. (3) The amount of the surface hydroxyl was increased. (4) The response range to light was expanded to the visible region [11]. These advantages of the Ag doped  $\text{TiO}_2$  nanofiber remarkably improved its photocatalytic performance. In other words, the greater increase of photocatalytic ability of Ag doped  $\text{TiO}_2$  nanofiber than that of pure  $\text{TiO}_2$  nanofiber must have contributed to effective separation of photogenerated electron–hole pairs in the anatase shell, which attributed to the facile injection of photogenerated electron into the doped silver.

We calculated the reaction rate constant by using a pseudo-first-order equation (Eq. 1), a simplified equation of Langmuir–Hinshelwood kinetic model (Eq. 2) [31, 32]

$$\ln\left(\frac{C_0}{C}\right) = kKt = k't \quad (1)$$

$$r = \frac{dC}{dt} = \frac{kKC}{1+KC} \quad (2)$$

where  $r$  is the rate of reaction ( $\text{mg L}^{-1} \text{ min}$ ),  $C_0$  is the initial concentration of MB ( $\text{mg L}^{-1}$ ),  $C$  is the concentration of the MB ( $\text{mg L}^{-1}$ ),  $t$  is the illumination time (min),  $k$  is the reaction rate constant ( $\text{min}^{-1}$ ), and  $K$  is the adsorption coefficient ( $\text{L mg}^{-1}$ ). From the results, we found the degradation rate of Ag doped  $\text{TiO}_2$  nanofiber was higher than that of  $\text{TiO}_2$  nanofiber.

From the experimental data of Fig. 6, we found to fit approximately a pseudo-first-order kinetic model by the

**Table 2** The removal efficiency of photocatalytic degradation by using  $\text{TiO}_2$  nanofiber and Ag doped  $\text{TiO}_2$  nanofiber about methylene blue

Sample name	Calcination temperature (°C)	Reaction temperature (°C)	Removal efficiency (%)
$\text{TiO}_2$ fiber	450	30	37
$\text{TiO}_2$ fiber	450	40	44
$\text{TiO}_2$ fiber	450	50	51
Ag doped $\text{TiO}_2$ fiber	450	30	60
Ag doped $\text{TiO}_2$ fiber	450	40	67
Ag doped $\text{TiO}_2$ fiber	450	50	76
$\text{TiO}_2$ fiber	500	30	55
$\text{TiO}_2$ fiber	500	40	62
$\text{TiO}_2$ fiber	500	50	69
Ag doped $\text{TiO}_2$ fiber	500	30	70
Ag doped $\text{TiO}_2$ fiber	500	40	74
Ag doped $\text{TiO}_2$ fiber	500	50	78

linear transforms. The values of the rate constant ( $k$ ) are listed in Table 2.

The first-order rate constant and activation energy of  $\text{TiO}_2$  nanofiber and Ag doped  $\text{TiO}_2$  nanofiber on photocatalytic degradation are listed in Table 3. The  $k$  (rate constant) increased as the temperature increased. Generally, increasing the reaction temperature enhances the reaction rate. The  $k$  values were adopted to calculate activation energy. The apparent activation energy was calculated by applying Arrhenius equation [33].

$$\ln(k) = \ln(A) - E_a/RT \quad (3)$$

where  $k$  is the rate constant of the pseudo-first-order model ( $\text{h}^{-1}$ ),  $A$  is the Arrhenius coefficient,  $E_a$  is activation energy (kJ/mol),  $R$  is the gas constant (8.314 J/mol K), and  $T$  is temperature (K).

For pure  $\text{TiO}_2$  nanofiber, activation energies of the calcination temperature of 450 and 500 °C are 16.981 and 12.374 kJ/mol. The activation energies of Ag doped  $\text{TiO}_2$  nanofiber at 450 and 500 °C were 18.137 and 7.977 kJ/mol. Also, the activation energy of photocatalyst sample with calcination temperature of 500 °C was relatively lower than of 450 °C.

## Conclusions

To prevent the recombination caused by the relatively low photocatalytic efficiency, Ag doped  $\text{TiO}_2$  nanofibers were prepared by the electrospinning method. The prepared photocatalysts (pure  $\text{TiO}_2$  nanofiber and Ag doped  $\text{TiO}_2$  nanofiber) were characterized by FE-SEM, XRD, XPS, and PL analysis. The surface of Ag doped  $\text{TiO}_2$  nanofiber is smoother than that of  $\text{TiO}_2$  nanofiber and the grain size the fiber is smaller. The pure  $\text{TiO}_2$  nanofiber has both anatase

**Table 3** First-order rate constant and activation energy of  $\text{TiO}_2$  nanofiber and Ag doped  $\text{TiO}_2$  nanofiber on photocatalytic degradation of methylene blue

Number (-)	Reaction temperature (°C)	First-order rate constant ( $k$ ) ( $\text{h}^{-1}$ )	Activation energy ( $E_a$ ) (kJ mol $^{-1}$ K $^{-1}$ )
$\text{TiO}_2$ fiber (450 °C)	30	0.1251	16.981
$\text{TiO}_2$ fiber (450 °C)	40	0.1559	
$\text{TiO}_2$ fiber (450 °C)	50	0.1898	
Ag doped $\text{TiO}_2$ fiber (450 °C)	30	0.2630	18.137
Ag doped $\text{TiO}_2$ fiber (450 °C)	40	0.3296	
Ag doped $\text{TiO}_2$ fiber (450 °C)	50	0.4106	
$\text{TiO}_2$ fiber (500 °C)	30	0.2244	12.374
$\text{TiO}_2$ fiber (500 °C)	40	0.2616	
$\text{TiO}_2$ fiber (500 °C)	50	0.3041	
Ag doped $\text{TiO}_2$ fiber (500 °C)	30	0.3460	7.977
Ag doped $\text{TiO}_2$ fiber (500 °C)	40	0.3813	
Ag doped $\text{TiO}_2$ fiber (500 °C)	50	0.4209	

phase and rutile phase, while Ag doped TiO<sub>2</sub> nanofiber has only the anatase phase. Ag doped TiO<sub>2</sub> nanofiber was found to be efficient than pure TiO<sub>2</sub> fiber at photocatalytic degradation of methylene blue. Compared to the pure TiO<sub>2</sub> fibers, the Ag doped TiO<sub>2</sub> nanofibers were found to be highly efficient for photocatalytic degradation of methylene blue. The activation energies for the pure TiO<sub>2</sub> nanofibers calcined at 400 and 500 °C were 16.981 and 12.187 kJ/mol and those of Ag doped TiO<sub>2</sub> nanofibers were 18.317 and 7.977 kJ/mol, respectively. In addition, the activation energy of photocatalyst sample with calcination temperature of 500 °C was relatively lower than of 450 °C.

## References

1. Sadek AZ, Partridge JG, McCulloch DG, Li YX, Yu XF, Włodarski W, Kalantar-zadeh K (2009) *Thin Solid Films* 518:1294
2. Steele JJ, Taschuk MT, Brett MJ (2009) *Sens Actuators B* 140:610
3. Ganapathy V, Karunagaran B, Rhee SW (2010) *J Power Source* 195:5138
4. Kim DH, Roy PM, Lee KY, Schmuki P (2010) *Electrochem Commun* 12:574
5. Wang S, Wu X, Qin W, Jiang Z (2008) *Mater Lett* 62:1078
6. Malagutti AR, Mourao HA, Garbin JR, Ribeiro C (2009) *Appl Catal B Environ* 90:205
7. Konstantinou IK, Albanis TA (2004) *Appl Catal B Environ* 49:1
8. Qu P, Zhao J, Shen T, Hidaka H (1998) *J Mol Catal A: Chem* 129:257
9. Libanori R, Giraldo TR, Longo E, Leite ER, Ribeiro C (2009) *J Sol-Gel Sci Technol* 49:95
10. Wang H, Wu Y, Xu BQ (2005) *Appl Catal B Environ* 59:139
11. Xin B, Jing L, Ren Z, Wang B, Fu H (2005) *J Phys Chem B* 109:2805
12. Chen Y, Sun Z, Yang Y, Ke Q (2001) *J Photochem Photobiol A* 142:85
13. Yang JC, Kim YC, Shul YG, Hin CH, Lee TK (1997) *Appl Surf Sci* 121:525
14. Chang CC, Chen JY, Hsu TL, Ling CK, Chan CC (2008) *Thin Solid Films* 516:1743
15. Colmenares JC, Aramendia MA, Marinas A, Marinas JM, Urbano FJ (2006) *Appl Catal A Gen* 306:120
16. Seery MK, George R, Floris P, Pillai SC (2007) *J Photochem Photobiol A* 189:258
17. Li D, Xia Y (2003) *Nano Lett* 3:555
18. Chuangchote S, Jitputti J, Sagawa T, Yoshikawa S (2009) *Appl Mater Interfaces* 1:1140
19. Nuansing W, Ninumuang S, Jarenboon W, Maensiri S, Seraphin S (2006) *Mater Sci Eng B* 131:147
20. Chandrasekar R, Zhang L, Howe JY, Hedin NE, Zhang Y, Fong H (2009) *J Mater Sci* 44:1198. doi:[10.1007/s10853-008-3201-1](https://doi.org/10.1007/s10853-008-3201-1)
21. He T, Zhou Z, Xu W, Ren F, Ma H, Wang J (2009) *Polymer* 50:3031
22. Alves AK, Berutti FA, Clemens FJ, Graule T, Bergmann CP (2009) *Mater Res Bull* 44:312
23. Doh SJ, Kim C, Lee SG, Lee SJ, Kim HY (2008) *J Hazard Mater* 154:118
24. Ding B, Kim HY, Kim CK, Khil MS, Park SJ (2003) *Nanotechnology* 14:532
25. Amores JMG, Escribano VS, Busca G (1995) *J Mater Chem* 5:1245
26. Amores JMG, Escribano VS, Busca G, Lorenzelli V (1994) *J Mater Chem* 4:965
27. Cho H, Yun YU, Xingfang HU, Larbot A (2003) *J Eur Ceram Soc* 23:1457
28. Cullity BD, Stock SR (2001) Elements of X-ray diffraction, 3rd edn. Prentice Hall, Upper Saddle River, NJ, pp 167–171
29. Zhang L, Mo CM (1995) *Nanostruct Mater* 6:831
30. Zhu YC, Ding CX (1999) *J Solid State Chem* 145:711
31. Pruden AL, Ollis DF (1983) *J Catal* 82:404
32. Ollis DF (1985) *Environ Sci Technol* 19:480
33. Wu CH, Yu CH (2009) *J Hazard Mater* 169:117